Investigation of CCN relevant properties and droplet growth kinetics of water-soluble aerosol fraction in Mexico City

Luz T. Padró[a], Daniel Tkacik[b+], Terry Lathem[b], Chris J. Hennigan[c,+], Amy P. Sullivan[b,‡], Rodney J. Weber[b], L. Greg Huey[b] and Athanasios Nenes[a,b,*]

[a]School of Chemical and Biomolecular Engineering, Georgia Institute of Technology, Atlanta, GA, USA

[b]School of Earth and Atmospheric Sciences, Georgia Institute of Technology, Atlanta, GA, USA

[c]School of Civil and Environmental Engineering, Georgia Institute of Technology, Atlanta, GA, USA

[+]Currently at the Center for Atmospheric Particle Studies, Carnegie Mellon University, Pittsburgh, PA

[‡]Currently at the Department of Atmospheric Science, Colorado State University, Fort Collins, CO

*Corresponding Author. Georgia Institute of Technology, School of Chemical and Biomolecular Engineering, 311 Ferst Dr. NW, Atlanta, GA, 30332, USA. Tel: + 1 404 894-9225;Fax: + 1 404 894 5638, athanasios.nenes@gatech.edu

Abstract

We present hygroscopic and CCN-relevant properties of the water-soluble fraction of Mexico City aerosol collected upon filters during the 2006 MILAGRO campaign. Application of κ- Köhler theory to the observed CCN activity gave a fairly constant hygroscopicity parameter (κ = 0.28 ± 0.06) regardless of location and organic fraction. Köhler theory analysis was used to understand this invariance by separating the molar volume and surfactant contributions to the CCN activity. Organics were found to depress surface tension (10-15%) from that of pure water. Daytime samples exhibited lower molar mass (~200 amu) and surface tension depression than nighttime samples (~400 amu); this is consistent with fresh hygroscopic secondary organic aerosol (SOA) condensing onto particles during peak photochemical hours, subsequently ageing during nighttime periods of high RH. Changes in surface tension partially compensates for shifts in average molar volume to give the constant hygroscopicity observed, which implies the amount (volume fraction) of soluble material in the parent aerosol is the key composition parameter required for CCN predictions. This finding, if applicable elsewhere, may explain why CCN predictions are often found to be insensitive to assumptions of chemical composition, and provides a very simple way to parameterize organic hygroscopicity in atmospheric models (i.e., $k_{org} = 0.3C_{\mathrm{WSOC}}$). Special care should be given however to surface tension depression from organic surfactants, as its nonlinear dependence with organic fraction may introduce biases in observed (and predicted) hygroscopicity. Finally, Threshold Droplet Growth analysis suggests the water-soluble organics do not affect activation kinetics.

Keywords: CCN, activation kinetics, organics, molar mass, activation

1 Introduction

It is well known that the ability of aerosols to act as cloud condensation nuclei (CCN) is a strong function of their size, chemical composition, and supersaturation levels in ambient clouds. The compositional complexity of aerosol, especially for the organic fraction, poses a challenge for its description in atmospheric models of aerosol-cloud interactions. Knowledge of their cumulative impact on CCN activity is nevertheless important, as carbonaceous material can constitute up to 90% of the total aerosol (e.g., Andreae and Crutzen, 1997; Moffet et al., 2008; Stone et al., 2008), 10-70% of which is water-soluble (Facchini et al., 2000; Hagler et al., 2007; Sullivan et al., 2004; Zappoli et al., 1999).

Many studies have focused on understanding the effects of water-soluble organic compounds on CCN activity (e.g., Asa-Awuku et al., 2008; Dinar et al., 2006b; Svenningsson et al., 2006), hygroscopicity (e.g., Badger et al., 2006; Brooks et al., 2004; Dinar et al., 2007; Svenningsson et al., 2006; Wex et al., 2007), droplet activation kinetics (e.g., Asa-Awuku et al., 2009; Engelhart et al., 2008; Ruehl et al., 2008; Ruehl et al., 2009) and surface tension (e.g., Asa-Awuku et al., 2008; Kiss et al., 2005; Taraniuk et al., 2007). Chemical characterization of the organics in ambient samples using analytical techniques such as size-exclusion chromatography and mass spectrometry (Kiss et al., 2003; Samburova et al., 2005; Zappoli et al., 1999) cannot identify the majority of compounds present. Even if complete speciation were possible, the amount of information produced is challenging to implement in models of aerosol-cloud interactions. Alternatively, indirect methods can be used to infer and parameterize the CCN properties of the organic fraction. Petters and Kreidenweis (2007) proposed the use

69 of a hygroscopicity parameter, κ (a parameterized Raoult term in Köhler theory), and is
70 being widely adopted to express the aerosol water uptake characteristics and CCN
71 activity of aerosol with a wide range of compositions. Wex et al. (2007) suggested
72 another single parameter approach, the ionic density, ρ_{ion}, to model the hygroscopic
73 growth of HUmic-LIke Substances (HULIS). Köhler Theory Analysis (KTA; Padró et al.,
74 2007; Asa-Awuku et al., 2007; Asa-Awuku et al., 2008; Moore et al., 2008; Engelhart et
75 al., 2008) uses measurements of size-resolved CCN activity and surface tension to infer
76 the molar volume of organics. In the absence of surface tension measurements, a form of
77 KTA can be applied to deconvolute the contribution of solute and surface tension
78 depression to the observed CCN activity (Moore et al., 2008; Asa-Awuku et al., 2009).
79 KTA is most successfully applied when the organic fraction in the aerosol is large and the
80 inorganic ion concentration and amount of water-soluble organic carbon (WSOC) is
81 known.

82 Studies to date using ambient data to constrain κ for organic aerosol often focus
83 on the value of the parameter, and less on the origin of the hygroscopicity (e.g., soluble
84 fraction, molar volume and surface tension depression). The latter is important, as κ,
85 when predicted in models, is calculated as the volume-fraction weighted average of the
86 hygroscopicity of each aerosol constituent. Surface tension effects do not obey "volume
87 additivity", so estimations of κ assuming a constant surface tension could be biased. For
88 example, Engelhart et al. (2008) found that κ ranged between 0.11 and 0.14 for secondary
89 organic aerosol (SOA) originating from monoterpene SOA. However, KTA of the water-
90 soluble fraction of the SOA suggests that ~60% of the aerosol is soluble, implying that
91 the true hygroscopicity parameter for the monoterpene SOA is 40% lower (i.e. κ =0.06-

92 0.084). The unaccounted ~ 10% surface tension reduction (with respect to pure water)
93 leads to the 40% overestimation of organic hygroscopicity. Surface tension reduction can
94 still be present even if the SOA is mixed with large amounts of electrolytes, so that the
95 aerosol would exhibit a higher hygroscopicity than expected from simple volume
96 additivity of κ.

97 In this study we characterize the CCN relevant properties (i.e., hygroscopicity
98 parameter, surface tension, molar volume, and droplet activation kinetics) of the water-
99 soluble fraction of Mexico City (MC) aerosol collected during March 2006. Emphasis is
100 placed on constraining the impact of water-soluble organics on droplet formation
101 (observing the activation kinetics and deconvoluting surface tension from solute
102 contributions to the hygroscopicity) and their temporal variation. Mexico City was
103 selected for sample collection as it represents an environment with strong anthropogenic
104 influences (e.g., biomass burning, fossil fuel, dust). Collection at two sites allows
105 comparison of aged/background properties against fresh emissions at downtown Mexico
106 City.

107

108 ## 2 Location description, sample collection, and experimental methods

109 ### 2.1 Location, meteorology, and air masses sampled

110 The main goal of MILAGRO (Megacity Initiative: Local and Global Research
111 Observations; http://www.eol.ucar.edu/projects/milagro/) was to study the evolution of
112 the Mexico City plume as it aged and quantify its impact on local and regional scales.
113 Mexico City was chosen owing to its size, pollution level, meteorology, and geography.
114 The field campaign took place in March, which is characterized by dry, clear sky

115 conditions with strong photochemistry (Jáuregui Ostos, 2000) and a low frequency of
116 biomass burning events. By selecting this period, the evolution of the Mexico City plume
117 could be studied without interference from regional biomass burning events (Fast et al.,
118 2007). Airborne and ground-based measurements were performed at three sites: *i*) the
119 "T0" site, at Instituto Mexicano de Petróleo (19.488° N, 99.147° W; Mexico City), *ii*) the
120 "T1" site, at the Universidad Tecnológica de Tecámac (19.703° N, 98.982° W; Tecámac,
121 Estado de México, Northeast of the city), and *iii*) the "T2" site, at Pachuca (20.010° N,
122 98.909° W). The design of the campaign and site selection was based on prevailing
123 meteorology and the MCMA-2003 campaign results (Molina et al., 2007). The T0 site
124 was chosen in the metropolitan area to represent fresh emissions while the T1 and T2
125 sites were chosen outside of the city limits to study the effects of transport mixing and
126 chemical aging on plume properties. Filter samples considered in this study were
127 collected at the T0 and T1 sites.

128 Three periods characterized the overall meteorological conditions throughout
129 MILAGRO (Fast et al., 2007). The first period was prior to March 14th, where clear sky
130 and dry conditions (relative humidity, RH < 50%) persisted. The second period (March
131 14th till the 23rd) was characterized by a sharp increase in RH (55 – 85%) and the
132 development of late afternoon convection associated with the passage of a weak cold
133 front on March 14th. The last and third period (after March 23rd) began with the passage
134 of a strong cold front which led to an increase in RH, afternoon convection, and stronger
135 precipitation events than those observed during the second period. As a result, the
136 frequency and intensity of fires within the vicinity of Mexico City during this period

diminished (Fast et al., 2007). Therefore, interaction between Mexico City and biomass burning plumes occurred mostly during the first 3 weeks of MILAGRO.

Tracer simulations using the WRF-Chem model suggest that the most direct transport between the T0 and T1 sites occurred from March 9 - 10 and March 18 – 20 (Fast et al., 2007). Further analysis of measurements and large scale analysis of the winds suggested favorable days of transport from T0 to T1 to have occurred during March 8 – 12, and, March 17 – 30 (Fast et al., 2007).

2.2 Particle collection and extraction

Ambient aerosols of aerodynamic diameter less than 2.5 μm ($PM_{2.5}$) were collected on quartz filters with Thermo Andersen Hi-Volume samplers. Three Hi-Volume samplers were used for aerosol collection: one located at T0 (on the rooftop of a building approximately 20 meters above ground level), and two located at ground level at the T1 site. Twenty-four and twelve hour integrated samples at T0 were collected from March 18 to 21, and from March 22 to 30, respectively. At T1, twenty-four hour samples were obtained from March 9 to 19, and twelve hour samples from March 20 to 30. At T1, twelve hour integrated samples were collected during daytime (6:00 to 18:00, Local Standard Time, LST) and nighttime (18:00 to 6:00, LST); only daytime samples were collected at T0. Aerosol collection for the twenty-four hour samples started at 10:00 LST at both locations.

The Hi-Volume samplers draw 1.16 m^3 min^{-1} of air over a two stage impactor assembly to separately collect particles from 10 – 2.5 μm and below 2.5 μm diameter. The quartz filters used in our study were pretreated to remove organic residue and excess

160 water vapor by baking them using the procedure of Sullivan and Weber (2006). After
161 particle collection in the field, the filters were stored in a freezer to limit losses of volatile
162 components until the WSOC is analyzed in the laboratory. Processing of the filter
163 samples involve extraction of the WSOC fraction in water. Since a high concentration
164 sample is needed to perform the surface tension measurements, multiple filters are
165 extracted at a time resulting in a sample with ~ 400 ppm of WSOC. Filters were grouped
166 by integration periods (Table 1) and placed in a Nalgene HDPE bottle with 125 mL of
167 dionized (DI) water for extraction. Two 24 hr filters were placed in each bottle, and three
168 for 12 hr filters. Each bottle was placed on a sonicator and heated in a water bath (with
169 temperature ~ 60°C; Baumann et al., 2003; Sullivan and Weber, 2006) for 75 minutes.
170 The solution was then allowed to cool down for 3 hours and filtered through a 0.45 μm
171 pore syringe filter to remove quartz fibers and insoluble particles suspended in solution.
172 The organic carbon concentration (C_{WSOC}) in all of the extracts was measured with a
173 Total Organic Carbon (TOC) analyzer (Section 2.3.1). The heating accelerates the
174 dissolution of the particles collected in the filter, while the cooling step allows the
175 repartitioning of semivolatile species back into solution. It is possible that some carbon
176 loss and chemical alterations of the sample may have occurred. Application of this
177 technique however to aerosol collected from chamber SOA experiments (Englehart et al.,
178 2008; Asa-Awuku et al., 2009) provided properties for the WSOC that is consistent with
179 known speciation. This suggests that water extraction may not substantially alter the
180 properties of the WSOC.

181 The Hi-Volume samplers used are not denuded making them susceptible to
182 positive artifacts from the absorption of organic vapors on the collected aerosols and

183 quartz filter fibers (Turpin et al., 1994; Sullivan and Weber, 2006). The extent of these
184 artifacts were assessed by Sullivan and Weber (2006), by comparing WSOC from online
185 (PILS-WSOC) and offline (filters) measurements similar to those presented in were
186 performed. WSOC concentrations from filter extracts were found to be about 20% higher
187 than the online measurements; therefore we are addressing an upper bound in amount of
188 water-soluble organics present in the aerosol.

189 Although grouping the filters allowed us to have enough mass for CCN
190 measurements, the extract was not concentrated enough for surface tension measurements
191 representative of CCN at the point of activation (1000 – 10000 ppm). This is addressed
192 by concentrating the samples using a rotary evaporator (rotavap; Büchi R-124), which
193 removes water with flash evaporization under vacuum and at ~75 °C. The water
194 evaporated from the sample is recondensed, while the concentrated WSOC solution
195 remains in the evaporation flask. A carbon balance calculation shows that most of the
196 WSOC (84 – 98%) remains in the concentrated sample.

197

198 **2.3 Chemical composition measurements**

199 2.3.1 TOC analyzer

200 WSOC concentration for all samples was measured with a portable TOC analyzer
201 (Sievers 900); organic carbon concentration is quantified in the sample by subtracting the
202 inorganic carbon concentration from the total carbon present. Inorganic and total carbon
203 concentration is determined by measuring the amount of carbon dioxide formed during
204 the acidification (for inorganic carbon) and oxidation (for total carbon) of the sample
205 streams. Prior to each measurement, samples were diluted by a factor of 250 or 1000 to

ensure the WSOC concentration lies within the dynamic range of the instrument (0.20 ppb to 10 ppm). Measurement of WSOC was repeated three times for each sample.

2.3.2 Ion chromatography

Ion chromatography (IC) was used to measure the concentration of the major ions in solution. The IC used in this study (Dionex Model DX500) has two channels, allowing for the measurement of anions and cations. An assessment of the instrument can be found in Butler (2000) and Cobb (2006). Anions measured included acetate ($C_2H_3O_2^-$), chloride (Cl^-), formate ($HCOO^-$), nitrate (NO_3^-), nitrite (NO_2^-), oxalate ($C_2O_4^{2-}$), and sulfate (SO_4^{2-}). The cations measured were ammonium (NH_4^+), calcium (Ca^{2+}), potassium (K^+), and sodium (Na^+). The samples were diluted by a factor of 50 to be within the dynamic range of the standards used for the IC calibration. The ion concentrations obtained from the IC measurement were then used as input for the ISORROPIA-II thermodynamic equilibrium code (Fountoukis and Nenes, 2007; http://nenes.eas.gatech.edu/ISORROPIA) to predict the mixture of inorganic salts dissolved in the samples (used in the application of KTA and κ-Köhler theory discussed in Section 3).

2.4 Surface tension

The surface tension of each sample was measured with a pendant drop tensiometer (CAM 200 Optical Contact Angle Meter, by KSV Inc.). A mechanically-controlled micro-syringe was used to produce a droplet of sample at the tip of a stainless steel needle. A picture of the drop is then taken at the point where the drop is ready to fall from the tip. The sample surface tension, σ, is then determined by fitting the droplet

229 shape to the Young-Laplace equation (Spelt and Li, 1996). Approximately 10 pictures per
230 droplet were taken to obtain an average and standard deviation for surface tension.

231 Surface tension depression depends on the surfactant concentration (expressed by
232 C_{WSOC}, the concentration of dissolved carbon), and is measured for each extract
233 concentration on the rotavap, and at 3:1, 2:1, 1:1, 1:3, and 1:∞ dilutions with ultrafine
234 pure water (Fisher). σ is then expressed against C_{WSOC} (ppm C; 1 ppm = 1 mg L^{-1} for a
235 solution of unit density) for each sample and fit to the Szyskowski-Langmuir equation
236 (Langmuir, 1917),

237 $$\sigma = \sigma_w - \alpha T \ln\left(1 + \beta C_{WSOC}\right) \quad (1)$$

238 where σ_w is the surface tension of water at temperature T of measurement, and the
239 parameters α and β are obtained by least squares minimization of Equation (1) to the
240 data.

241

242 **2.5 Measurements of CCN activity and droplet activation kinetics**

243 The laboratory setup employed to characterize the CCN activity of the dissolved
244 material and the impact of organic material on the droplet activation kinetics is described
245 in Padró et al. (2007) and Asa-Awuku et al. (2008). The system consists of an aerosol
246 generation, size classification, and CCN measurement section. Polydisperse aerosols are
247 generated by atomizing the filter extracts. The droplets are subsequently dried by flowing
248 them through multiple diffusion driers and charged with a Kr-85 bipolar charger (TSI
249 Model 3077). A Differential Mobility Analyzer (DMA, TSI Model 3081L) is then used
250 for size mobility selection of the dry particles. The classified aerosol flow is split into two

streams, one sent to a Condensation Particle Counter (CPC, TSI Model 3022A) to measure their concentration (CN) and the other to a Continuous Flow Streamwise Thermal Gradient CCN Chamber (CFSTGC, Lance et al., 2006; Roberts and Nenes, 2005) to measure the fraction that act as CCN. The activated droplets in the CCN are counted and sized at the exit with an Optical Particle Counter (OPC, 660 nm) with a dynamic range of 0.75 to 10 μm with 0.5 μm bin resolution.

In this work, CCN activation data is obtained using Scanning Mobility CCN Analysis (SMCA; Nenes et al., in review[1]; Asa-Awuku et al., 2009; Moore et al., 2008); instead of "stepping" through the DMA voltage to obtain CCN concentrations at discrete values of mobility diameter, the DMA voltage is continuously changed over time, so that the dynamic mobility range of the DMA is "scanned" over 2 min. During a size scan, the supersaturation in the CFSTGC is maintained constant. The time series of activated droplet size, CCN, and CN counts are then inverted to obtain size-resolved CCN activity and activation kinetics. In this study, the aerosol size was ranged between 7 and 260 nm, and 0.2% to 1.2% supersaturation.

CCN activity of the aerosol is characterized by determining the minimum dry diameter, d_{p50}, of particles that activate into cloud droplets at each supersaturation (i.e., those particles with a critical supersaturation equal to the instrument supersaturation). d_{p50} is found by expressing the ratio of CCN to CN concentration with respect to dry particle diameter and determining the dry diameter for which 50% of the aerosol act as CCN. To facilitate the analysis, the activation data is fit to a sigmoid curve which neglects the impact of multiply-charged particles; d_{p50} then corresponds to the inflection point of the

[1]Nenes A., Moore, R. and Medina J. Scanning Mobility CCN Analysis – A method for fast measurements of size-resolved CCN distributions and activation kinetics, Aerosol Science and Technology, *in review*

sigmoid. Once the d_{p50} at each supersaturation is known, a "CCN spectrum" (s_c versus d_{p50}) can be obtained and used to characterize the average properties of WSOC using Köhler Theory Analysis or κ-Köhler Theory (Section 3).

The CCN instrument used in this study was calibrated with $(NH_4)_2SO_4$ using a procedure similar to that of Sorooshian et al., (2008), Asa-Awuku et al., (2009), and Rose et al., (2008). The calibration procedure consisted of generating particles by atomizing a $(NH_4)_2SO_4$ solution. The polydisperse aerosol was then dried, charged, and size selected with a DMA operated in scanning voltage mode. The effective supersaturation in the column was determined from d_{p50} using traditional Köhler theory, with osmotic coefficients calculated with the Pitzer activity coefficient model (Clegg and Brimblecombe, 1988; Pitzer and Mayorga, 1973) and the surface tension of water (calculated at the average column temperature). The uncertainty in supersaturation was determined from Köhler theory and the standard deviation observed in the d_{p50}. This procedure is repeated for multiple values of ΔT, for which calibration curves of instrument supersaturation versus ΔT are generated. The resulting calibration curves are shown in Figure 1.

CCN activation kinetics and changes thereof from the presence of organics can also be determined from the CCN measurements. This is done by monitoring the droplet size measured at the OPC for particles of critical supersaturation equal to the instrument supersaturation (i.e., dry diameter equal to d_{p50}). For particles composed of pure deliquescent electrolytes (e.g., $(NH_4)_2SO_4$ calibration aerosol), CCN activation kinetics is rapid (corresponding to an uptake coefficient of ~ 0.1) and the wet droplet size, D_w, corresponding to the d_{p50} particles is used as a reference (for the given conditions of

pressure, ΔT, and flow). Comparing D_w against the corresponding wet diameter (i.e. same critical supersaturation) of activated particles generated from the extracted filters can reveal whether organic compounds retard activation kinetics. This technique, called "Threshold Droplet Growth Analysis (TDGA)", has been successfully applied to a number of in-situ (Sorooshian et al., 2008; Bougiatioti et al., 2009; Murphy et al., 2009; Lance et al., 2009) and laboratory (Moore et al., 2008; Engelhart et al., 2008; Asa-Awuku et al., 2007, 2009) studies. When combined with a computational fluid dynamics model of the CCN instrument (Lance et al., 2006), changes in droplet size can then be parameterized in terms of changes in the water vapor uptake coefficient (Asa-Awuku et al., 2009; Engelhart et al., 2008; Ruehl et al., 2008; Ruehl et al., 2009).

2.6 Effects of electrolyte addition on surface tension and CCN activity

The presence of inorganic solute at high concentrations may enhance the presence of organics at the droplet-air interface and affect surface tension (Asa-Awuku et al., 2008; Kiss et al., 2005). To explore this potential, prescribed amounts of $(NH_4)_2SO_4$, m_{AS}, as multiples of the existing organic mass, is added to the sample:

$$m_{AS} = f m_{org} \quad (2)$$

where f is the "mass addition factor", m_{org} is the mass of dissolved organic matter in the sample (mg), given by $m_{org} = \left[\frac{OM}{OC}\right] C_{WSOC} V_{sample}$, V_{sample} is the sample volume (L), and OM/OC is the organic matter-to-organic carbon ratio, assumed 1.5 for T0 and 2.3 for T1, respectively (DeCarlo et al., 2008; Aiken et al., 2008). Different OM/OC values are used at each site since to reflect the oxidation state of the aerosol at each location. Lower

318 OM/OC ratios correspond to fresher emissions (at T0) while larger values to aged
319 regional air (at T1).
320
321 ## 3 Experimental analysis
322 ### 3.1 Köhler theory analysis
323 Köhler Theory Analysis is used to infer average thermodynamic properties (e.g.,
324 molar volume) of the water-soluble organic fraction of the aerosol. The method is based
325 on combining Köhler theory with size-resolved CCN, chemical composition, and surface
326 tension measurements (Padró et al., 2007). When combined with SMCA (Nenes and et
327 al., in review[1]), KTA allows the characterization of the CCN relevant properties of
328 ambient WSOC from small amount of sample typically collected on filters. KTA has
329 been evaluated for laboratory generated particles composed of inorganic-organic
330 mixtures of known composition (Padró et al., 2007), biomass burning WSOC (Asa-
331 Awuku et al., 2008), secondary organic aerosol (Asa-Awuku et al., 2009; Asa-Awuku et
332 al., 2007; Engelhart et al., 2008) and primary marine organic matter (Moore et al., 2008).
333 According to KTA, the average molar volume, $\frac{M_{org}}{\rho_{org}}$, of the soluble organic
334 fraction of an aerosol is given by,
335 $$\frac{M_{org}}{\rho_{org}} = \frac{\varepsilon_{org}\upsilon_{org}}{\frac{256}{27}\left(\frac{M_w}{\rho_w}\right)^2\left(\frac{1}{RT}\right)^3\sigma^3\omega^{-2} - \sum_{inorg}\left(\frac{\rho}{M}\right)_{inorg}\varepsilon_{inorg}\upsilon_{inorg}} \quad (3)$$
336 where M_{org}, ε_{org}, υ_{org}, ρ_{org} is the molar mass, dry volume fraction, effective van't Hoff
337 factor, and density of the organic fraction, respectively; M_{inorg}, ρ_{inorg}, ε_{inorg}, and υ_{inorg} are

the molecular weight, density, volume fraction, and effective van't Hoff factor of the inorganic compounds present in the aerosol sample (Table 2), respectively. M_w and ρ_w are the molar mass and density of water, respectively, R is the ideal gas constant, T is the temperature, and σ is the surface tension of the solution at the point of activation. The Pitzer activity coefficient model (Clegg and Brimblecombe, 1988; Pitzer and Mayorga, 1973) is used to calculate the effective υ_{inorg} for all inorganic salts present in the samples, at the concentration corresponding to the critical wet diameter of the CCN (Padró et al., 2007). ω is the "Fitted CCN Activity" (FCA) parameter (Padró et al., 2007), obtained by expressing CCN activity measurements by the power-law expression $s_c = \omega d_{50}^{-3/2}$. The volume fraction of substance "i", ε_i, is computed as follows:

$$\varepsilon_i = \frac{x_i/\rho_i}{\sum_j (x/\rho)_j} \quad (4)$$

where x_i is the mass fraction of the compound of interest, and j refers to all compounds present in the aerosol (organic or inorganic; Tables 3 and 4). The ionic composition of each sample (obtained from the IC) is converted into a mixture of salts by applying the ISORROPIA-II model as described in section 2.3.2. *OM* is assumed to have 1.6 g cm^{-3} density (Dinar et al., 2006a) at T0 and a 1.5 g cm^{-3} density at T1 (Cross et al., 2009).

The uncertainty in the inferred organic molar mass, ΔM_{org}, can be estimated from the total uncertainty from each parameter as:

$$\Delta M_{org} = \sqrt{\sum (\Phi_z \Delta z)^2} \quad (5)$$

where Φ_z is the sensitivity of the organic molar mass to a parameter, z, that affects M_{org} (i.e., σ, ω, υ_{org}, υ_{inorg}, ε_{org}, and ε_{inorg}), $\Phi_z = \frac{\partial M_{org}}{\partial z}$, and Δz is the uncertainty on z. The formulas used to compute the sensitivity of the organic molar mass to z are shown in Table 5.

3.2 κ-Köhler theory analysis

κ-Köhler theory was introduced by Petters and Kreidenweis (2007) to represent aerosol hygroscopic water uptake and CCN activity through the "hygroscopicity parameter", κ, that collectively accounts for density, molar mass, and dissociation effects of solute on water activity (the "Raoult term" in the Köhler equation). κ values range from 0.0 to 2, with hygroscopic inorganic species such as $(NH_4)_2SO_4$ and NaCl having κ ranging from 0.5 to 2 and organic species and mixtures ranging from 0.01 to 0.5. For $\kappa >$ 0.01, "simple" Köhler theory applies and the hygroscopicity parameter can be obtained from s_c and d_{p50} pairs as

$$\kappa = \frac{4A^3}{27 d_{p50}^3 s_c^2} \quad (6)$$

where $A = \frac{4M_w \sigma_w}{RT\rho_w}$ and s_c is the instrument supersaturation. κ is calculated using the surface tension of water evaluated at the median column temperature (Petters and Kreidenweis, 2007).

Surface tension of the CCN can be different from water if surfactants (e.g., HULIS) are present (Dinar et al., 2007; Kiss et al., 2005). This can introduce notable

uncertainty in κ calculations, the extent of which can be evaluated from Equation (6). If the surface tension depression from pure water at the point of activation is $\Delta\sigma$, then the true value of κ is a factor of $\left(1-\frac{\Delta\sigma}{\sigma_w}\right)^3$ lower. For example, for a 10 % depression ($\Delta\sigma/\sigma_w$ = 0.10), κ is ~30% lower than the values inferred when the surface tension of pure water is assumed.

4 Results and discussion

4.1 Surfactant characteristics

Table 6 presents the fitted Szyskowski-Langmuir adsorption constants α and β (Equation (1)), the maximum C_{WSOC} of the extracted and concentrated sample, and the concentration of SO_4^{2-} ions in solution (C_{SO4}). The surface tension depression is also presented at C_{WSOC} = 1000 ppm for comparison purposes. Even though organics at both locations depress σ, stronger depression is seen at T0 (24 hr samples, Figure 2a; 12 hr day samples, Figure 2b) consistent with having a higher hydrophobic fraction (lower O/C ratio) very near emission sources (DeCarlo et al., 2008; Kleinman et al., 2008). The observed surface tension depression at the T0 site (for both sample periods) could further be enhanced by the higher salt concentration present at this site, as suggested by the enhanced surface tension depression seen in the salted samples (Table 6).

Differences were observed in surfactant characteristics between the day and night samples at T1, with nighttime samples being slightly more surface active than the day samples (Figure 2c). Higher σ depression observed in the nighttime samples may reflect influence from primary emissions (which tend to be more hydrophobic than SOA

399 produced during the daytime), or, ageing of hygroscopic SOA (formed during daytime
400 photochemical production) in the aqueous phase to form HULIS (Hoffer et al., 2004). A
401 source apportionment study performed for the fine organic aerosol for T0 and T1 sites
402 found particulates at T1 to be influenced by local sources rather than from the Mexico
403 City outflow (Stone et al., 2008).
404
405 **4.2 CCN activity and hygroscopicity**
406 The CCN activity (embodied in the s_c versus d_{p50} relationship) of aerosol
407 generated from some of the extracted samples is presented in Figure 3. The curves shown
408 are grouped by sites and integration period (Figures 3a and b) as well as the time of day
409 for the T1 samples (Figure 3c). As a first approximation, the extracts were found to have
410 similar CCN activity regardless of the site (Figures 3a and b). Compared to T1 samples,
411 T0 samples tend to have somewhat higher CCN activity (i.e., the s_c-d_{p50} curve is closer to
412 that of $(NH_4)_2SO_4$) due to the stronger surface tension depression and the higher salt
413 fraction in the latter samples (Tables 3 and 4). The CCN activity of 12 hr (day and night)
414 samples collected at T1 (Figure 3c) presents little variability.
415 κ was calculated from application of Equation (6) to the s_c and d_{p50} pairs (Table 1).
416 For the T0 site samples, κ ranged between 0.29 – 0.32 (24 hr filters) and 0.25 – 0.39 (12
417 hr filters). κ for the T1 site samples ranged from 0.30 – 0.37 (24 hr filters), 0.21 – 0.26
418 (12 hr day filters), and 0.22 – 0.28 (12 hr night filters). The overall average is 0.28 ±
419 0.06. These values of κ are consistent with soluble salts and very hygroscopic organics
420 (Carrico et al., 2008; Koehler et al., 2009; Petters and Kreidenweis, 2007; Shantz et al.,
421 2008). κ values obtained at the T1 site are also consistent with those derived from

422 concurrent in-situ CCN measurements (Lance, 2007; Table 1), indicating that the
423 material obtained from the filter water extraction reflects the hygroscopic properties of
424 the ambient aerosol. Given that the aerosol from filter extracts is completely soluble, one
425 expected that its κ will be higher than the in-situ (parent) aerosol. Indeed this is the case
426 (Lance, 2007; Table 1). No significant correlation was found between κ and the organic
427 mass fraction or sampling site (Figure 4; $R^2 = 0.01$).

428 The invariance of κ with respect to soluble organic fraction although counterintuitive,
429 provides insight on the nature of the WSOC. First, the water-soluble components
430 extracted from both sites have about the same hygroscopicity, suggesting that ageing
431 processes may not affect its overall hygroscopicity (although their detailed speciation
432 may vary considerably) but only their relative amount in the aerosol. Second, the
433 hygroscopicity of the water-soluble organic (i.e., κ for $x_{org} \rightarrow 1$) and inorganic fractions
434 (i.e., κ for $x_{org} \rightarrow 0$) are very similar (Figure 4); this invariance may reflect a
435 compensation between solute (when $x_{org} \rightarrow 0$) and surface tension depression (when χ_{org}
436 $\rightarrow 1$) effects. Also, $\kappa \rightarrow 0.4$ for $x_{org} \rightarrow 0$ (Figure 4), which is somewhat lower than values
437 for mixtures of electrolytes (~0.6 and above). This is likely because the inorganic fraction
438 is predicted to contain a fair amount of $CaSO_4$ and $CaCO_3$ that dissolves completely
439 during the water extraction process, but to a much lesser degree in the limited amounts of
440 water in CCN at their critical wet diameter (Tables 2, 3 and 4).
441

442 **4.3 Average organic molecular weight**

443 KTA is used to infer the average organic molar volume based on Equation (3),
444 measured surface tension (Table 6), FCA factor, and chemical composition (Tables 3 and

4). During application of KTA, υ_{org} is assumed ~ 1. For most of the samples collected at T1, an excess of cations (Ca^{2+}, Na^{+}, and K^{+}) was present and correlated with dust; excess Ca^{2+} is assumed bound to CO_3^{-}, while excess K^{+} and Na^{+} is associated with re-suspension of dry lake bed salt from Lake Texcoco (Vega et al., 2001, located southwest of the T1 site). Metereological data (de Foy et al., 2008; Fast et al., 2007) support this, since on these dates a high pressure system present over the Gulf of Mexico caused southwesterly winds over the MC area that favored the transport of salt-rich dust from the dry lake bed to the site. To verify that the composition predicted by ISORROPIA-II is representative of the salt mixture in the filter samples, we compared the predicted hygroscopicity of the inorganic fraction with the measured hygroscopicity of samples with an organic fraction approaching zero. Predicted κ at T1 is in the range of 0.3-0.4 (Table 4), which agrees with the observations (Table 2 and Figure 4).

The organic mass fraction in the T0 site samples was low where KTA is subject to large uncertainty (Padró et al., 2007). Hence molar mass estimates are calculated only for T1 site samples where the organic mass fraction is larger than 50% (Padró et al., 2007, i.e., all samples except T1-5 and T1-7). The molar volumes inferred from KTA when multiplied by the organic density, ρ_{org}, gives an estimation of the organic molecular weight (Table 1). Higher molecular weight organics were found for the 12 hr samples (330 amu on average for day and night) relative to the 24 hr samples (149 amu on average). The 12 hr samples were collected during the third period, which were characterized by high relative humidity and evening rain events, which did not occur in the previous period (before March 23; de Foy et al., 2008; Fast et al., 2007). Under such conditions, the formation of higher-molecular weight compounds through condensed-

468 phase chemistry is favored. With the exception of a high O_3 event on March 22, diurnal
469 changes in gas phase oxidant levels (O_3 and OH) did not vary substantially during the
470 period, hence not likely responsible for this change (Case Hanks, 2008). Increases in
471 sulfur dioxide (SO_2) were however observed from March 21-27, associated with transport
472 from the Tula power plant (de Foy et al., 2009); the enhanced RH during this time period,
473 combined with increases in aerosol acidity and sulfate could promote the formation of
474 high molecular weight compounds through a variety of mechanisms, such as acid-
475 catalyzed reactions (e.g., Jang et al., 2002; Edney et al., 2005; Surratt et al., 2007),
476 reactive uptake of volatile aldehydes or ketones via peroxyhemiacetal formation (Tobias
477 et al., 2000; Docherty et al., 2005), hydration, hemiacetal/acetal formation, and aldol
478 condensation (Jang et al., 2001; Jang et al., 2002). For the T1 12 hr samples, a lower
479 organic molecular weight (~ 290 amu on average) was inferred for the day samples
480 (Table 1), consistent with condensation of fresh SOA during peak photochemical activity;
481 subsequent reactions in the condensed phase would tend to increase the average
482 molecular weight of the organics at night. This is consistent with oxygenated organic
483 matter dominating the carbonaceous fraction in afternoon and evening periods (de Gouw
484 et al., 2009). The diurnal profile of size-resolved CCN activity measurements carried out
485 during the same time period (Lance et al., 2007) support this view (although the in-situ
486 data exhibit a 30-50% lower κ, likely because not all of the aerosol volume is water-
487 soluble).
488
489
490

4.4 Sensitivity analysis and hygroscopicity parameter closure

A sensitivity analysis was performed to determine the greatest source of uncertainty in the organic molar mass calculations. Of the six parameters considered (σ, ω, υ_{org}, υ_{inorg}, ε_{org}, and ε_{inorg}), the greatest source of uncertainty arises from the effective van't Hoff factor, followed by the FCA parameter. The total estimated uncertainty in molar mass for all the samples is ~ 20% (Table 7) similar to levels estimated in other KTA studies (e.g., Asa-Awuku et al., 2007, Asa-Awuku et al., 2008, Asa-Awuku et al., 2009; Englehart et al., 2008; Moore et al., 2008; Padró et al., 2007).

A "κ closure" analysis was also performed to compare the predicted (κ_{mix}) and measured (κ_{CCN}) hygroscopicity parameter values. κ_{CCN} was determined from the s_c and d_{p50} pairs as detailed in Section 3.2. κ_{mix} was calculated by applying a mixing rule to the aerosol composition (Petters and Kreidenweis, 2007),

$$\kappa_{mix} = \sum_i \varepsilon_i \kappa_i \tag{7}$$

where κ_i is the hygroscopicity parameter of component i,

$$\kappa_i = \frac{M_w \rho_i \upsilon_i}{\rho_w M_i} \tag{8}$$

κ for the water-soluble organic fraction was calculated using the properties determined by KTA (Section 4.3). κ for salts potentially present in the extracted filters are presented in Table 2. κ_{CCN} is sensitive to the assumption of surface tension used (Equation (6)), and is evaluated by assuming: *i*) the surface tension of water and *ii*) 15% surface tension from the contribution of organics (an expected value, based on Figures 2a and b). It should be

511 pointed out that κ_{mix} is still affected by the surface tension used for calculating M_{org}
512 during application of KTA.

513 The κ_{mix}-κ_{CCN} closure (Figure 5) shows that neglecting the effects of surface
514 tension depression of organics leads to a 40% underestimation of κ. When κ_{CCN} is
515 calculated allowing for a 15% surface tension depression, excellent closure is obtained
516 between predictions and measurements. This implies that neglecting surfactant
517 characteristics of the aerosol can result in a substantial overestimation of organic
518 hygroscopicity (even if inorganic salts exist in the particles), which could be important
519 for predictions of CCN concentrations and subsaturated water uptake if substantial
520 amounts of hygroscopic organics are present in the aerosol.

521

522 **4.5 CCN activation kinetics**

523 The impact of water-soluble organics on the CCN activation kinetics was studied
524 using TDGA, which is based on comparing D_w from the sample CCN against that of
525 $(NH_4)_2SO_4$ calibration aerosol. If the droplet sizes from ambient aerosols are smaller than
526 those from calibration aerosol (with same s_c and for identical conditions of instrument
527 operation), the activation kinetics are said to be affected by organics. However, if
528 activated droplet sizes are indistinguishable (to within experimental uncertainty) from
529 $(NH_4)_2SO_4$ data, they are said to exhibit rapid activation kinetics.

530 Activated droplet sizes obtained for the pure Mexico City samples at both sites
531 (12 hr day integration) are shown in Figure 6; droplet sizes are indistinguishable from
532 $(NH_4)_2SO_4$, hence the water-soluble organics present in the Mexico City samples do not
533 retard activation kinetics. However, activation kinetics of *in-situ* CCN performed at T1
534 can be retarded, particularly during periods of lower hygroscopicity at midday (Lance,

2007). All together, this data suggests that any observed retardations in activation kinetics will be associated with the insoluble fraction. This is consistent with knowledge to date (e.g., Asa-Awuku et al. 2007; Moore et al. 2008; Engelhart et al. 2008; Sorooshian et al. 2008;Asa-Awuku et al. 2009; Murphy et al. 2009; Bougiatioti et al., 2009).

5 Conclusions

Ambient aerosols were collected with Hi-Volume samplers on March 2006 during the MILAGRO field campaign in Mexico City. Particles were collected at the T0 (downtown) and T1 (northeast of the city) sites. 12 and 24 hr filter samples were collected to contrast daytime versus nighttime characteristics. Characterization of the water-soluble fraction was done by measuring its CCN activity, growth kinetics, surface tension, and ionic composition. Köhler Theory Analysis (Padró et al., 2007) was used to infer the average molecular weight of the organics by coupling it to parameters obtained from the offline analysis methods employed here. κ -Köhler theory analysis was also carried out to examine the variability of the soluble mass hygroscopicity and its sensitivity to the surfactant characteristics of the particulate matter.

From our analysis, we found the water-soluble organics present in Mexico City act as surfactants; surface tension depression was stronger at T0 than at T1, possibly due to more hydrophobic organics present in the former (fresh emissions), further promoted by higher salt concentrations. The most unexpected result is that the water-soluble fraction, regardless of sampling site and period, exhibit remarkably similar CCN activity and hygroscopicity. KTA analysis of the samples suggests that the invariance in κ are a result of changes in molar volume being compensated by surface tension depression. The constant value of κ implies that the CCN activity of the parent aerosol depends solely on

its soluble fraction (inorganic and organic combined) and its dry particle diameter. When closure in predicted κ is attempted, neglecting the effects from surfactants may lead to a 50% discrepancy, which is present even if most of the water-soluble fraction is inorganic. Given that this overprediction corresponds to a 15% surface tension depression (which is not atypical for CCN containing surfactants), studies that use a κ-based approach to parameterize compositional impacts on CCN activity need to account for this variability (at least as a sensitivity calculation). Application of KTA to the T1 site samples suggests that the organic molar mass varies between night and day samples by twofold (220 to 430 amu), exhibiting the lowest molar mass during the day. The observed increase in molar mass during the nighttime is consistent with local primary emissions condensing upon the particles, combined with aqueous reactions that could form HULIS. Finally, the activation kinetics of CCN formed from the water-soluble material was found to be similar to $(NH_4)_2SO_4$.

In conclusion, this study suggests that the water-soluble fraction of aerosol as complex as that found in Mexico City exhibits constant hygroscopicity, $\kappa = 0.28 \pm 0.06$, over a wide range of organic mass fraction. Köhler theory analysis of the samples suggests that changes in surface tension may compensate for shifts in average molar volume to give the constant hygroscopicity observed, which implies the amount (volume fraction) of soluble material in the parent aerosol is the key composition parameter required for CCN predictions. This finding, if applicable elsewhere, may explain why CCN predictions are often found to be insensitive to assumptions of chemical composition (e.g., Dusek et al., 2006; Vestin et al., 2007), and provides a very simple way to parameterize organic hygroscopicity in atmospheric models (which for WSOC

582 can be described as $k_{org} = 0.28\varepsilon_{WSOC}$). Special care should be given however to surface
583 tension depression from organic surfactants, as its nonlinear dependence with organic
584 fraction may introduce biases in predicted hygroscopicity.

Acknowledgements

This research was supported in part by a NSF CAREER, a NOAA ACC, and a NASA ESS award. This work was partially supported by NSF ATM 0513035. We would like to thank M. Bergin and G. Hagler (Georgia Institute of Technology) for use of their Turbo Siever 900 TOC analyzer and Büchi rotavapor. We also thank A. G. Russell and E. Cobb (Georgia Institute of Technology) for the use of the Dionex Ion Chromatograph for chemical characterization.

References

Aiken, A. C., P. F. DeCarlo, J. H. Kroll, D. R. Worsnop, J. A. Huffman, K. S. Docherty, I. M. Ulbrich, C. Mohr, J. R. Kimmel, D. Sueper, Y. Sun, Q. Zhang, A. Trimborn, M. Northway, P. J. Ziemann, M. R. Canagaratna, T. B. Onasch, M. R. Alfarra, A. S. H. Prevot, J. Dommen, J. Duplissy, A. Metzger, U. Baltensperger and J. L. Jimenez, O/C and OM/OC ratios of primary, secondary, and ambient organic aerosols with high-resolution-time-of-flight aerosol mass spectrometry, *Environmental Science & Technology*, *42*, 4478 - 4485, 2008.

Andreae, M. O. and P. J. Crutzen, Atmospheric Aerosols: Biogeochemical Sources and Role in Atmospheric Chemistry, *Science*, *276*, 1052-1058, 1997.

Asa-Awuku, A., A. Nenes, S. Gao, R. C. Flagan and J. H. Seinfeld, Alkene ozonolysis SOA: inferences of composition and droplet growth kinetics from Köhler theory analysis, *Atmospheric Chemistry and Physics Discussions*, *7*, 8983-9011, 2007.

Asa-Awuku, A., A. Nenes, A. P. Sullivan, C. Hennigan and R. J. Weber, Investigation of Molar Volume and Surfactant Characteristics of Water-Soluble Organic Compounds in Biomass Burning Aerosol *Atmospheric Chemistry and Physics*, *8*, 799 - 812, 2008.

Asa-Awuku, A., G. J. Engelhart, B. H. Lee, S. N. Pandis and A. Nenes, Relating CCN activity, volatility, and droplet growth kinetics of β-caryophyllene secondary organic aerosol, *Atmospheric Chemistry and Physics*, *9*, 795-812, 2009.

Badger, C. L., I. George, P. T. Griffiths, C. F. Braban, R. A. Cox and J. P. D. Abbatt, Phase transitions and hygroscopic growth of aerosol particles containing humic acid and mixtures of humic acid and ammonium sulphate, *Atmospheric Chemistry and Physics*, *6*, 755-768, 2006.

Baumann, K., F. Ift, J. Z. Zhao and W. L. Chameides, Discrete measurements of reactive gases and fine particle mass and composition during the 1999 Atlanta Supersite Experiment, *Journal of Geophysical Research*, *108*, 8416, doi:10.1029/2001JD001210, 2003.

Bougiatioti, A., C. Fountoukis, N. Kalivitis, S. N. Pandis, A. Nenes and N. Mihalopoulos, Cloud condensation nuclei measurements in the eastern Mediterranean marine boundary layer: CCN closure and droplet growth kinetics, *Atmospheric Chemistry and Physics*, *9*, – 7053 - 7066, 2009.

623 Brooks, S. D., P. J. DeMott and S. M. Kreidenweis, Water uptake by particles containing
624 humic materials and mixtures of humic materials with ammonium sulfate, *Atmospheric*
625 *Environment*, *38*, 1859-1868, 2004.

626 Butler, A. J., Temporal and spatial analysis of PM2.5 mass and composition in Atlanta,
627 School of Civil and Environmental Engineering, Atlanta, Georgia Institute of
628 Technology. **Doctor of Philosophy**, 2000.

629 Carrico, C. M., M. D. Petters, S. M. Kreidenweis, J. L. Collett, G. Engling and W. C.
630 Malm, Aerosol hygroscopicity and cloud droplet activation of extracts of filters from
631 biomass burning experiments, *Journal of Geophysical Research-Atmospheres*, *113*,
632 D08206, doi:10.1029/2007JD009274, 2008.

633 Case Hanks, A. T., Formaldehyde instrument development and boundary layer sulfuric
634 acid: implications for photochemistry, School of Earth and Atmospheric Sciences,
635 Atlanta, GA, Georgia Institute of Technology, **Doctor of Philosophy**, 2008.

636 Clegg, S. L. and P. Brimblecombe, Equilibrium partial pressures of strong acids over
637 concentrated saline solutions -- I. HNO3., *Atmospheric Environment*, *1*, 91-100, 1988.

638 Cobb, C. E., Spatial and temporal variations of PM2.5 mass and composition in Atlanta:
639 ASACA 1999 – 2006, School of Civil and Environmental Engineering, Atlanta, Georgia
640 Institute of Technology, **Master of Science**, 2006.

641 Cross, E. S., T. B. Onasch, M. Canagaratna, J. T. Jayne, J. Kimmel, X.-Y. Yu, M. L.
642 Alexander, D. R. Worsnop and P. Davidovits, Single particle characterization using a
643 light scattering module coupled to a time-of-flight aerosol mass spectrometer,
644 *Atmospheric Chemistry and Physics, 9,* 7769-7793, 2009.

645 Cross, E. S., T. B. Onasch, M. Canagaratna, J. T. Jayne, J. Kimmel, X.-Y. Yu, M. L.
646 Alexander, D. R. Worsnop and P. Davidovits, Single particle characterization using a
647 light scattering module coupled to a time-of-flight aerosol mass spectrometer,
648 *Atmospheric Chemistry and Physics, 9,* 7769-7793, 20099.

649 de Foy, B., J. D. Fast, S. J. Paech, D. Phillips, J. T. Walters, R. L. Coulter, T. J. Martin,
650 M. S. Pekour, W. J. Shaw, P. P. Kastendeuch, N. A. Marley, A. Retama and L. T.
651 Molina, Basin-scale wind transport during the MILAGRO field campaign and
652 comparison to climatology using cluster analysis, *Atmospheric Chemistry and Physics*, *8*,
653 1209-1224, 2008.

de Gouw, J. A., D. Welsh-Bon, C. Warneke, W. C. Kuster, L. Alexander, A. K. Baker, A. J. Beyersdorf, D. R. Blake, M. Canagaratna, A. T. Celada, L. G. Huey, W. Junkermann, T. B. Onasch, A. Salcido, S. J. Sjostedt, A. P. Sullivan, D. J. Tanner, O. Vargas, R. J. Weber, D. R. Worsnop, X. Y. Yu and R. Zaveri, Emission and chemistry of organic carbon in the gas and aerosol phase at a sub-urban site near Mexico City in March 2006 during the MILAGRO study, *Atmospheric Chemistry and Physics*, *9*, 3425 - 3442, 2009.

DeCarlo, P. F., E. J. Dunlea, J. R. Kimmel, A. C. Aiken, D. Sueper, J. Crounse, P. O. Wennberg, L. Emmons, Y. Shinozuka, A. Clarke, J. Zhou, J. Tomlinson, D. R. Collins, D. Knapp, A. J. Weinheimer, D. D. Montzka, T. Campos and J. L. Jimenez, Fast Airborne Aerosol Size and Chemistry Measurements with the High Resolution Aerosol Mass Spectrometer during the MILAGRO Campaign, *Atmospheric Chemistry and Physics*, *8*, 4027 - 4048, 2008.

Dinar, E., T. F. Mentel and Y. Rudich, The density of humic acids and humic like substances (HULIS) from fresh and aged wood burning and pollution aerosol particles, *Atmospheric Chemistry and Physics*, *6*, 5213-5224, 2006a.

Dinar, E., I. Taraniuk, E. R. Graber, S. Katsman, T. Moise, T. Anttila, T. F. Mentel and Y. Rudich, Cloud Condensation Nuclei properties of model and atmospheric HULIS, *Atmospheric Chemistry and Physics*, *6*, 2465-2482, 2006b.

Dinar, E., I. Taraniuk, E. R. Graber, T. Anttila, T. F. Mentel and Y. Rudich, Hygroscopic growth of atmospheric and model humic-like substances, *Journal of Geophysical Research - Atmospheres*, *112*, D05211, doi:10.1029/2006JD007442, 2007.

Docherty, K. S., W. Wu, Y. B. Lim and P. J. Ziemann, Contributions of organic peroxides to secondary aerosol formed from reactions of monoterpenes with O-3, *Environmental Science & Technology*, *39*, 11, 4049-4059, 2005.

Dusek, U., G. P. Reischl and R. Hitzenberger, CCN activation of pure and coated carbon black particles, *Environmental Science & Technology*, *40*, 4, 1223-1230, 2006.

Edney, E. O., T. E. Kleindienst, M. Jaoui, M. Lewandowski, J. H. Offenberg, W. Wang and M. Claeys, Formation of 2-methyl tetrols and 2-methylglyceric acid in secondary organic aerosol from laboratory irradiated isoprene/NOX/SO2/air mixtures and their detection in ambient PM2.5 samples collected in the eastern United States, *Atmospheric Environment*, *39*, 29, 5281-5289, 2005.

685 Engelhart, G. J., A. Asa-Awuku, A. Nenes and S. N. Pandis, CCN activity and droplet
686 growth kinetics of fresh and aged monoterpene secondary organic aerosol, *Atmospheric*
687 *Chemistry and Physics*, *8*, 3937 - 3949, 2008.

688 Facchini, M. C., S. Decesari, M. Mircea, S. Fuzzi and G. Loglio, Surface tension of
689 atmospheric wet aerosol and cloud/fog droplets in relation to their organic carbon content
690 and chemical composition, *Atmospheric Environment*, *34*, 28, 4853-4857, 2000.

691 Fast, J. D., B. De Foy, F. Acevedo Rosas, E. Caetano, G. Carmichael, L. Emmons, D.
692 McKenna, M. Mena, W. Skamarock, X. Tie, R. L. Coulter, J. C. Barnard, C. Wiedinmyer
693 and S. Madronich, A meteorological overview of the MILAGRO field campaigns,
694 *Atmospheric Chemistry and Physics 7*, 2233-2257, 2007.

695 Fountoukis, C. and A. Nenes, ISORROPIA II: a computationally efficient
696 thermodynamic equilibrium model for K^+ -Ca^{2+} -Mg^{2+} -$NH4^+$ -Na^+ -SO_4^{2-} -NO_3^- -Cl^- -
697 H_2O aerosols, *Atmospheric Chemistry and Physics*, *7*, 4639-4659, 2007.

698 Hagler, G. S. W., M. H. Bergin, E. A. Smith and J. E. Dibb, A summer time series of
699 particulate carbon in the air and snow at Summit, Greenland, *Journal of Geophysical*
700 *Research - Atmospheres*, *112, D21309*, doi:10.1029/2007JD008993, 2007.

701 Hoffer, A., G. Kiss, M. Blazso and A. Gelencser, Chemical characterization of humic-
702 like substances (HULIS) formed from a lignin-type precursor in model cloud water,
703 *Geophysical Research Letters*, *31*, 2004.

704 Jang, M. S. and R. M. Kamens, Atmospheric secondary aerosol formation by
705 heterogeneous reactions of aldehydes in the presence of a sulfuric acid aerosol catalyst,
706 *Environmental Science & Technology*, *35*, 24, 4758-4766, 2001.

707 Jang, M. S., N. M. Czoschke, S. Lee and R. M. Kamens, Heterogeneous atmospheric
708 aerosol production by acid-catalyzed particle-phase reactions, *Science*, *298*, 5594, 814-
709 817, 2002.

710 Jáuregui Ostos, E., *El clima de la Ciudad de México*, México, D.F., Instituto de
711 Geografía – UNAM, 2000.

712 Kiss, G., E. Tombacz, B. Varga, T. Alsberg and L. Persson, Estimation of the average
713 molecular weight of humic-like substances isolated from fine atmospheric aerosol,
714 *Atmospheric Environment*, *37*, 27, 3783-3794, 2003.

715 Kiss, G., E. Tombacz and H. C. Hansson, Surface tension effects of humic-like
716 substances in the aqueous extract of tropospheric fine aerosol, *Journal of Atmospheric*
717 *Chemistry*, *50*, 3, 279-294, 2005.

718 Kleinman, L. I., S. R. Springston, P. H. Daum, Y.-N. Lee, L. J. Nunnermacker, G. I.
719 Senum, J. Wang, J. Weinstein-Lloyd, M. L. Alexander, J. Hubbe, J. Ortega, M.
720 Canagaratna and J. Jayne, The time evolution of aerosol composition over the Mexico
721 City plateau, *Atmospheric Chemistry and Physics*, *8*, 1559-1575, 2008.

722 Koehler, K. A., S. M. Kreidenweis, P. J. DeMott, M. D. Petters, A. J. Prenni and C. M.
723 Carrico, Hygroscopicity and cloud droplet activation of mineral dust aerosol,
724 *Geophysical Research Letters*, *36*, L08805, doi:10.1029/2009GL037348, 2009.

725 Lance, S., J. Medina, J. N. Smith and A. Nenes, Mapping the operation of the DMT
726 continuous flow CCN counter *Aerosol Science and Technology*, *40*, 242-254, 2006.

727 Lance, S., Quantifying compositional impacts of ambient aerosol on cloud droplet
728 formation, School of Earth and Atmospheric Sciences, Atlanta, Georgia Institute of
729 Technology, **Doctor of Philosophy**, 2007.

730 Lance, S., A. Nenes, C. Mazzoleni, M. Dubey, H. Gates, V. Varutbangkul, T. A.
731 Rissman, S. M. Murphy, A. Sorooshian, F. Brechtel, R.C. Flagan, J.H. Seinfeld, G.
732 Feingold and H. Jonsson, CCN Activity, Closure and Droplet Growth Kinetics of
733 Houston Aerosol During the Gulf of Mexico Atmospheric Composition and Climate
734 Study (GoMACCS), *Journal of Geophysical Research*, *114*, D00F15,
735 doi:10.1029/2008JD011699, 2009.

736 Langmuir, I., The constitution and fundamental properties of solids and liquids. II.
737 Liquids., *Journal of the American Chemical Society*, *39*, 1848-1906, 1917.

738 Moffet, R. C., B. de Foy, L. T. Molina, M. J. Molina and A. Prather, Measurement of
739 ambient aerosols in northern Mexico City by single particle mass spectrometry,
740 *Atmospheric Chemistry and Physics*, *8*, 4499-4516, 2008.

741 Molina, L. T., C. E. Kolb, B. de Foy, B. R. Lamb, W. H. Brune, J. L. Jimenez, R. Ramos-
742 Villegas, J. Sarmiento, V. H. Paramo-Figueroa, B. Cardenas, B. Gutierrez-Avedoy and
743 M. J. Molina, Air quality in North America's most populous city – overview of the
744 MCMA-2003 campaign, *Atmospheric Chemistry and Physics, 7,* 2447-2473, 2007.

745 Moore, R. H., E. D. Ingall, A. Sorooshian and A. Nenes, Molar mass, surface tension,
746 and droplet growth kinetics of marine organics from measurements of CCN activity,
747 *Geophysical Research Letters*, *35*, L07801, doi:10.1029/2008GL033350, 2008.

748 Murphy, S. M., H. Agrawal, A. Sorooshian, L. T. Padro, H. Gates, S. Hersey, W. A.
749 Welch, H. Jung, J. W. Miller, D. R. Cocker III, A. Nenes, H. H. Jonsson, R. C. Flagan
750 and J. H. Seinfeld, Comprehensive simultaneous shipboard and airborne characterization
751 of exhaust from a modern container ship at sea, *Environmental Science & Technology*,
752 doi:10.1021/es802413j, 2009.

753 Padró, L. T., R. Morrison, A. Asa-Awuku and A. Nenes, Inferring Thermodynamic
754 Properties from CCN Activation Experiments: Single-component and Binary Aerosols,
755 *Atmospheric Chemistry and Physics*, *7*, 5263 - 5274, 2007.

756 Petters, M. D. and S. M. Kreidenweis, A single parameter representation of hygroscopic
757 growth and cloud condensation nucleus activity, *Atmospheric Chemistry and Physics*, *7*,
758 1961-19711, 2007.

759 Pitzer, K. S. and G. Mayorga, Thermodynamics of electrolytes -- II. Activity and osmotic
760 coefficients for strong electrolytes with one or both ions univalent, *Journal of Physical*
761 *Chemistry*, *77*, 2300-2308, 1973.

762 Roberts, G. C. and A. Nenes, A continuous-flow streamwise thermal-gradient CCN
763 chamber for atmospheric measurements, *Aerosol Science and Technology*, *39*, 3, 206-
764 211, 2005.

765 Rose, D., G. P. Frank, U. Dusek, S. S. Gunthe, M. O. Andreae and U. Pöschl, Calibration
766 and measurement uncertainties of a continuous-flow cloud condensation nuclei counter
767 (DMT-CCNC): CCN activation of ammonium sulfate and sodium chloride aerosol
768 particles in theory and experiment, *Atmospheric Chemistry and Physics*, *8*, 1153-1179,
769 2008.

770 Ruehl, C. R., P. Y. Chuang and A. Nenes, How quickly do cloud droplets form on
771 atmospheric particles?, *Atmospheric Chemistry and Physics*, *8*, 1043 - 1055, 2008.

772 Ruehl, C. R., P. Y. Chuang and A. Nenes, Distinct CCN activation kinetics above the
773 marine boundary layer along the California coast, *Geophysical Research Letters*, *36*,
774 L15814, doi:10.1029/2009GL038839, 2009.

775 Samburova, V., R. Zenobi and M. Kalberer, Characterization of high molecular weight
776 compounds in urban atmospheric particles, *Atmospheric Chemistry and Physics*, *5*, 2163-
777 2170, 2005.

778 Shantz, N. C., W. R. Leaitch, L. Phinney, M. Mozurkewich and D. Toom-Sauntry, The
779 effect of organic compounds on the growth rate of cloud droplets in marine and forest
780 settings, *Atmospheric Chemistry and Physics*, *8*, 5869-5887, 2008.

781 Sorooshian, A., S. M. Murphy, S. Hersey, H. Gates, L. T. Padro, A. Nenes, F. J. Brechtel,
782 H. Jonsson, R. C. Flagan and J. H. Seinfeld, Comprehensive airborne characterization of
783 aerosol from a major bovine source, *Atmospheric Chemistry and Physics*, *8*, 5489 - 5520,
784 2008.

785 Spelt, J. K. and D. Li (1996). Applied Surface Thermodynamics. New York, Marcel
786 Dekker.

787 Stone, E. A., D. C. Snyder, R. J. Sheesley, A. P. Sullivan, R. J. Weber and J. J. Schauer,
788 Source apportionment of fine organic aerosol in Mexico City during the MILAGRO
789 Experiment 2006, *Atmospheric Chemistry and Physics*, *8*, 1249-1259, 2008.

790 Sullivan, A. P., R. J. Weber, A. L. Clements, J. R. Turner, M. S. Bae and J. J. Schauer, A
791 method for on-line measurement of water-soluble organic carbon in ambient aerosol
792 particles: Results from an urban site, *Geophysical Research Letters*, *31, L13105*,
793 doi:10.1029/2004GL019681, 2004.

794 Sullivan, A. P. and R. J. Weber, Chemical characterization of the ambient organic aerosol
795 soluble in water: 2. Isolation of acid, neutral, and basic fractions by modified size-
796 exclusion chromatography, *Journal of Geophysical Research-Atmospheres*, *111*, D5, Art.
797 No. D05315, doi:10.1029/2005JD006486, 2006.

798 Surratt, J. D., J. H. Kroll, T. E. Kleindienst, E. O. Edney, M. Claeys, A. Sorooshian, N. L.
799 Ng, J. H. Offenberg, M. Lewandowski, M. Jaoui, R. C. Flagan and J. H. Seinfeld,
800 Evidence for organosulfates in secondary organic aerosol, *Environmental Science &*
801 *Technology*, *41*, 517-527, 2007.

802 Svenningsson, B., J. Rissler, E. Swietlicki, M. Mircea, M. Bilde, M. C. Facchini, S.
803 Decesari, S. Fuzzi, J. Zhou, J. Monster and T. Rosenorn, Hygroscopic growth and critical
804 supersaturations for mixed aerosol particles of inorganic and organic compounds of
805 atmospheric relevance, *Atmospheric Chemistry and Physics 6*, 1937-1952, 2006.

806 Taraniuk, I., E. R. Graber, A. Kostinski and Y. Rudich, Surfactant properties of
807 atmospheric and model humic-like substances (HULIS), *Geophysical Research Letters*,
808 *34*, L16807, doi:10.1029/2007GL029576, 2007.

809 Tobias, H. J. and P. J. Ziemann, Thermal desorption mass spectrometric analysis of
810 organic aerosol formed from reactions of 1-tetradecene and O-3 in the presence of
811 alcohols and carboxylic acids, *Environmental Science & Technology*, *34*, 11, 2105-2115,
812 2000.

813 Vega, E., V. Mugica, E. Reyes, G. Sánchez, J. C. Chow and J. G. Watson, Chemical
814 composition of fugitive dust emitters in Mexico City, *Atmospheric Environment*, *35*,
815 4033-4039, 2001.

816 Vestin, A., J. Rissler, E. Swietlicki, G. P. Frank and M. O. Andreae, Cloud-nucleating
817 properties of the Amazonian biomass burning aerosol: Cloud condensation nuclei
818 measurements and modeling, *Journal of Geophysical Research - Atmospheres*, *112*,
819 D14201, doi:10.1029/2006JD008104, 2007.

820

821 Wex, H., T. Hennig, I. Salma, R. Ocksay, A. Kiselev, S. Henning, A. Massling, A.
822 Wiedensohler and F. Stratmann, Hygroscopic growth and measured and modeled critical
823 supersaturations of an atmospheric HULIS sample, *Geophysical Research Letters*, *34*,
824 L02818,doi:10.1029/2006GL028260, 2007.

825 Zappoli, S., A. Andracchio, S. Fuzzi, M. C. Facchini, A. Gelencser, G. Kiss, Z. Krivacsy,
826 A. Molnar, E. Meszaros, H. C. Hansson, K. Rosman and Y. Zebuhr, Inorganic, organic
827 and macromolecular components of fine aerosol in different areas of Europe in relation to
828 their water solubility, *Atmospheric Environment*, *33*, 17, 2733-2743, 1999.

Figure Captions

Figure 1: Instrument supersaturation versus delta T. Calibration was performed at a flowrate of 500 cm^3 min^{-1} and at ambient pressure using $(NH_4)_2SO_4$ aerosol.

Figure 2: Surface tension as a function of concentration for (a) 24 hour integrated samples: MEX-T0-1 (◆), MEX-T0-2 (■), MEX-T1-1 (▲), and MEX-T1-2 (●), (b) 12 hr integration day samples: MEX-T0-4 (◆), MEX-T0-5 (■), MEX-T1-11 (▲), and MEX-T1-12 (●), (c) 12 hr integration night samples: MEX-T1-8 (◆), MEX-T1-9 (■), and 12 hr integration day samples: MEX-T1-11 (▲), and MEX-T1-12 (●). The solid lines correspond to the Szyskowski-Langmuir fit for each sample.

Figure 3: CCN activity for (a) 24 hour integrated samples: MEX-T0-1 (◆), MEX-T0-2 (■), MEX-T1-1 (▲), and MEX-T1-2 (●), (b) 12 hr integration day samples: MEX-T0-3 (◆), MEX-T0-4 (■), MEX-T1-11 (▲), and MEX-T1-12 (●), (c) 12 hr integration night samples: MEX-T1-8 (◆), MEX-T1-9 (■), and 12 hr integration day samples: MEX-T1-11 (▲), and MEX-T1-12 (●) with their corresponding power fit) assuming complete solubility. $(NH_4)_2SO_4$ (■) is also shown for comparison.

Figure 4: Hygroscopicity parameter versus organic mass fraction: T0 24 hr (red open square), T0 12 hr day (red open circle), T1 24 hr (blue open square), T1 12 hr day (blue open circle), T1 12 hr night (blue open triangle). The black dotted line represents the hygroscopicity parameter for $(NH_4)_2SO_4$.

Figure 5: Hygroscopicity parameter closure plot for T1 extracted samples. Comparison of κ_{mix} and κ_{CCN} assuming the surface tension of water (blue diamonds) and 15% surface tension depression (pink squares). The black dashed line represents the 1 to 1 line. The red dotted-dashed lines define the 50% error range.

Figure 6: Activated droplet sizes for particles of dry diameter equal to d_{p50}. Results shown for aerosol collected from 12 hr integration day samples: MEX-T0-3 (◆), MEX-T0-4 (■), MEX-T1-11 (▲), MEX-T1-12 (●), and $(NH_4)_2SO_4$ (■). Grey area denotes sizing uncertainty for $(NH_4)_2SO_4$.

866 Table 1. Summary of filter grouping with extracted WSOC concentration (C_{WSOC}),
867 inferred average organic molecular weight (M_{org}), and hygroscopicity parameter (κ).
868 Also shown also κ derived from concurrent in-situ aerosol measurements (Lance, 2007).

869

Sample Name (sample period)	Collection Date (March)	C_{WSOC} (ppm)	M_{org} (g mol^{-1})	*In-situ* κ[b]	κ_{CCN}[c]
MEX-T0-1 (24 hr)	18 - 19	287.5 ± 1.44	N/A[a]	N/A[d]	0.319 ± 0.055
MEX-T0-2 (24 hr)	20 - 21	310 ± 0	N/A[a]	N/A[d]	0.288 ± 0.073
MEX-T0-3 (12 hr day)	22 - 24	246.25 ± 0.43	N/A[a]	N/A[d]	0.271 ± 0.046
MEX-T0-4 (12 hr day)	25 - 27	715 ± 5.2	N/A[a]	N/A[d]	0.252 ± 0.019
MEX-T0-5 (12 hr day)	28 - 30	237.75 ± 3.08	N/A[a]	N/A[d]	0.290 ± 0.107
MEX-T1-1 (24 hr)	9, 11	392.5 ± 1.44	158.31 ± 56.41	N/A[d]	0.339 ± 0.094
MEX-T1-2 (24 hr)	13, 16	317.5 ± 1.44	141.81 ± 11.73	~ 0.25	0.316 ± 0.052
MEX-T1-3 (24 hr)	17 - 18	115.5 ± 0.95	161.92 ± 11.79	~ 0.30	0.329 ± 0.024
MEX-T1-4 (24 hr)	15 - 16	217 ± 0.63	222.71 ± 15.67	~ 0.25	0.297 ± 0.029
MEX-T1-5 (24 hr)	17 - 18	110.5 ± 0.80	N/A[a]	0.25 – 0.30	0.311 ± 0.025
MEX-T1-6 (24 hr)	19	117.5 ± 2.5	61.93 ± 6.18	~ 0.30	0.366 ± 0.017
MEX-T1-7 (12 hr night)	20 - 22	114.5 ± 0.72	N/A[a]	~ 0.20	0.220 ± 0.017
MEX-T1-8 (12 hr night)	23 - 25	76.75 ± 3.48	431.35 ± 210.28	~ 0.20	0.221 ± 0.023
MEX-T1-9 (12 hr night)	26 -28	140.75 ± 1.42	344.64 ± 117.61	N/A[d]	0.275 ± 0.030
MEX-T1-10 (12 hr day)	21 - 23	382.5 ± 1.44	380.82 ± 97.00	0.20 – 0.25	0.214 ± 0.013
MEX-T1-11 (12 hr day)	24 - 26	352.5 ± 1.44	221.97 ± 8.08	~ 0.25	0.263 ± 0.010
MEX-T1-12 (12 hr day)	27 - 29	362.5 ± 1.44	267.89 ± 13.94	N/A[d]	0.256 ± 0.006

870 [a]organic mass fraction insufficiently high for application of KTA.
871 [b]obtained from *in-situ* CCN activity measurements of 100 nm aerosol at T1 (Lance, 2007).
872 [c]calculated by application of Equation 6, assuming the surface tension of water.
873 [d]CCN measurements not available at location or time.

874 Table 2. Properties of inorganic salts potentially present in the extracted filters.

875

Compound Name	Chemical Formula	Molar mass (g mol^{-1})	ρ[a] (g cm^{-3})	κ
Ammonium Bisulfate	NH_4HSO_4	115.11	1.79	0.53
Ammonium Chloride	NH_4Cl	53.49	2.165	1.46
Ammonium Nitrate	NH_4NO_3	80.04	1.5	0.64
Ammonium Sulfate	$(NH_4)_2SO_4$	132.14	1.77[b]	0.60
Calcium Carbonate	$CaCO_3$	100.09	2.71	< 0.01
Calcium Chloride	$CaCl_2$	110.98	2.15	0.70
Calcium Nitrate	$Ca(NO_3)_2$	164	1.82	0.40
Calcium Sulfate	$CaSO_4$	136.14	2.32	< 0.01
Letovicite	$(NH_4)_3H(SO_4)_2$	247.25	1.83	0.60
Potassium Bisulfate	$KHSO_4$	136.17	2.24	0.59
Potassium Sulfate	K_2SO_4	174.27	2.66	0.69
Sodium Bisulfate	$NaHSO_4$	120.06	2.742	0.82
Sodium Sulfate	Na_2SO_4	142.04	2.68	0.85
Sulfuric Acid	H_2SO_4	98.08	1.84	0.81

876 [a]Unless noted values are from the Material Safety Data Sheet.
877 [b]Svenningsson et al. (2006).
878

879

880 Table 3. Organic and inorganic mass fraction for Mexico City T0 site samples. Salts shown for each sample were predicted by using
881 ISORROPIA II (Fountoukis and Nenes, 2007). Uncertainties in all mass fractions are less than 0.3%.

882

Sample	x_{org}	$x_{Na_2SO_4}$	x_{NaHSO_4}	$x_{(NH_4)_2SO_4}$	$x_{NH_4HSO_4}$	$x_{(NH_4)_3H(SO_4)_2}$	x_{CaSO_4}	$x_{K_2SO_4}$	x_{KHSO_4}	$x_{H_2SO_4}$	κ_{inorg}
MEX-T0-1	0.22	0	0.21	0	0.29	0	0.11	0	0.02	0.16	0.593
MEX-T0-2	0.27	0	0.19	0	0.30	0	0.10	0	0.02	0.12	0.576
MEX-T0-3	0.25	0.07	0.13	0	0.41	0	0.11	0.03	0	0	0.525
MEX-T0-4	0.55	0.11	0	0.13	0	0.12	0.08	0.02	0	0	0.555
MEX-T0-5	0.35	0.17	0	0.36	0	0	0.10	0.02	0	0	0.573

883

884

885

886

887

888

889

890

891

Table 4. Organic and inorganic mass fraction for Mexico City T1 site samples. Salts shown for each sample were predicted by using ISORROPIA II (Fountoukis and Nenes, 2007). Uncertainties in all mass fractions are smaller than 0.3%.

Sample	x_{org}	$x_{(NH_4)_2SO_4}$	$x_{NH_4NO_3}$	x_{NH_4Cl}	x_{CaSO_4}	$x_{Ca_2(NO_3)_2}$	x_{CaCl_2}	$x_{Na_2CO_3}$	x_{CaCO_3}	$x_{K_2CO_3}$	$x_{Na_2SO_4}$	$x_{K_2SO_4}$	κ_{inorg}	κ_{org}
MEX-T1-1	0.72	0.08	0	0	0.10	0	0	0.02	0	0	0.06	0.03	0.415	0.171
MEX-T1-2	0.67	0.12	0	0	0.06	0	0	0.06	0.08	0.02	0	0	0.264	0.190
MEX-T1-3	0.49	0.17	0	0	0.02	0	0	0.07	0.21	0.04	0	0	0.255	0.167
MEX-T1-4	0.57	0.12	0.03	0.02	0	0	0	0.07	0.16	0.03	0	0	0.331	0.121
MEX-T1-5	0.39	0.21	0.01	0	0	0.06	0	0.12	0.17	0.04	0	0	0.314	N/A[a]
MEX-T1-6	0.44	0.12	0	0	0.14	0	0	0.17	0.09	0.06	0	0	0.157	0.436
MEX-T1-7	0.50	0.14	0.05	0	0	0.01	0	0.16	0.11	0.03	0	0	0.305	N/A[a]
MEX-T1-8	0.52	0.09	0.02	0	0	0.02	0	0.20	0.11	0.02	0	0	0.212	0.063
MEX-T1-9	0.59	0.09	0.06	0.01	0	0	0.03	0.17	0.04	0.02	0	0	0.352	0.078
MEX-T1-10	0.70	0.09	0.02	0	0	0.01	0	0.10	0.07	0.02	0	0	0.290	0.071
MEX-T1-11	0.68	0.06	0.04	0.01	0	0	0.003	0.14	0.07	0.01	0	0	0.282	0.122
MEX-T1-12	0.74	0.06	0.05	0	0	0	0.01	0.09	0.04	0.01	0	0	0.360	0.101

[a]organic mass fraction insufficiently high for application of KTA.

Table 5. Formulas used for computing the sensitivity of molar volume to σ, ω, υ_{org}, υ_{inorg}, ε_{org}, and ε_{inorg}.

Parameter, z	Sensitivity, $\Phi_z = \frac{\partial M_{org}}{\partial z}$
σ	$\Phi_\sigma = \frac{768}{27}\left(\frac{M_w}{\rho_w}\right)^2\left(\frac{1}{RT}\right)^3\frac{\sigma^2 M_{org}^2}{\varepsilon_{org}\upsilon_{org}\rho_{org}\omega^2}$
ω	$\Phi_\omega = \frac{512}{27}\left(\frac{M_w}{\rho_w}\right)^2\left(\frac{1}{RT}\right)^3\frac{\sigma^3 M_{org}^2}{\varepsilon_{org}\upsilon_{org}\rho_{org}\omega^3}$
υ_{org}	$\Phi_{\upsilon_{org}} = \frac{256}{27}\left(\frac{M_w}{\rho_w}\right)^2\left(\frac{1}{RT}\right)^3\frac{\sigma^3 M_{org}^2}{\varepsilon_{org}\rho_{org}\upsilon_{org}^2\omega^2} + \frac{M_{org}^2}{\varepsilon_{org}\rho_{org}\upsilon_{org}^2}\left(\sum_{inorg}\left(\frac{\rho_{inorg}}{M_{inorg}}\right)\varepsilon_{inorg}\upsilon_{inorg}\right)$
υ_{inorg} [a]	$\Phi_{\upsilon_{inorg}} = \left(\frac{\rho_{inorg}}{M_{inorg}}\right)\frac{\varepsilon_{inorg}M_{org}^2}{\varepsilon_{org}\rho_{org}\upsilon_{org}}$
ε_{org}	$\Phi_{\varepsilon_{org}} = \frac{256}{27}\left(\frac{M_w}{\rho_w}\right)^2\left(\frac{1}{RT}\right)^3\frac{\sigma^3 M_{org}^2}{\upsilon_{org}\rho_{org}\varepsilon_{org}^2\omega^2} + \frac{M_{org}^2}{\upsilon_{org}\rho_{org}\varepsilon_{org}^2}\left(\sum_{inorg}\left(\frac{\rho_{inorg}}{M_{inorg}}\right)\varepsilon_{inorg}\upsilon_{inorg}\right)$
ε_{inorg} [a]	$\Phi_{\varepsilon_{inorg}} = \left(\frac{\rho_{inorg}}{M_{inorg}}\right)\frac{\upsilon_{inorg}M_{org}^2}{\varepsilon_{org}\upsilon_{org}\rho_{org}}$

[a] Inorganics potentially present at T0 are: Na_2SO_4, $NaHSO_4$, $(NH_4)_2SO_4$, NH_4HSO_4, $(NH_4)_3H(SO_4)_2$, $CaSO_4$, K_2SO_4, $KHSO_4$, and $H2SO_4$
Inorganics potentially present at T1 are: $(NH_4)_2SO_4$, NH_4NO_3, NH_4Cl, $CaSO_4$, $Ca(NO_3)_2$, $CaCl_2$, Na_2CO_3, $CaCO_3$, K_2CO_3, Na_2SO_4, and K_2SO_4.

906 Table 6. Constants from fitting the surface tension measurements of pure and salted (with
907 $(NH_4)_2SO_4$) filter extracts to the Szyskowski-Langmuir equation (298 K).

Sample Name (C_{WSOC} [a])	Mixture with $(NH_4)_2SO_4$, f	C_{SO4} (ppm)	$\alpha \times 10^1$ (mN m^{-1}K^{-1})	$\beta \times 10^5$ (ppm^{-1})	Surface Tension Depression[b] (%)
MEX-T0-1	0	1320	8.22	6.35	21.93
(1030 ppm)	1.333	2956	2.29	24.7	21.91
	12	15060	2.64	22.9	23.59
MEX-T0-2	0	1066	6.39	6.68	17.91
(995 ppm)	1.333	2629	3.99	11.8	19.29
	12	14188	3.38	14.8	20.22
MEX-T0-3	0	893	5.09	5.17	11.12
(686 ppm)	1.333	1947	6.26	5.83	15.37
	12	10162	12.20	3.77	19.57
MEX-T0-4	0	654	5.18	4.97	10.89
(896 ppm)	1.333	1999	2.93	8.27	10.09
	12	12322	6.28	4.90	13.02
MEX-T0-5	0	342	5.84	5.43	13.38
(604 ppm)	1.333	996	4.95	5.70	11.89
	12	8120	2.98	11.6	14.18
MEX-T1-1	0	235	3.33	6.92	9.66
(578 ppm)	0.870	1071	2.60	8.83	9.54
	7.826	7795	3.34	8.26	11.49
MEX-T1-2	0	140	4.74	6.06	12.09
(433 ppm)	0.870	467	1.50	16.9	10.15
	7.826	2975	1.51	8.99	5.63
MEX-T1-3	0	74	2.32	9.34	8.98
(465 ppm)	0.870	765	1.14	19.7	8.89
	7.826	6144	6.00	4.10	10.45
MEX-T1-4	0	76	1.47	18.2	10.65
(365 ppm)	0.870	621	1.95	9.92	7.99
	7.826	4837	9.24	4.39	17.21
MEX-T1-5	0	101	1.44	19.5	11.12
(300 ppm)	0.870	538	1.29	13.8	7.23
	7.826	4027	1.28	19.7	9.98
MEX-T1-6	0	116	0.037	2400	5.16
(451 ppm)	0.870	770	3.60	5.25	7.98
	7.826	6004	0.44	50.9	7.85
MEX-T1-7	0	54	3.39	3.40	4.91
(348 ppm)	0.870	563	3.93	3.38	5.66
	7.826	4598	5.43	5.23	12.00
MEX-T1-8	0	22	5.62	3.89	9.30
(227 ppm)	0.870	349	5.80	5.18	12.70
	7.826	3003	3.61	8.46	12.71
MEX-T1-9	0	35	4.37	4.22	7.83
(296 ppm)	0.870	471	2.09	8.60	7.47
	7.826	3924	3.23	7.04	9.52
MEX-T1-10	0	78	14.9	1.85	11.84
(850 ppm)	0.870	1314	5.45	5.04	11.62
	7.826	11201	9.09	2.66	10.34
MEX-T1-11	0	56	3.58	5.66	8.54
(345 ppm)	0.870	565	3.58	7.02	10.53
	7.826	4563	2.58	8.78	9.41
MEX-T1-12	0	48	4.46	4.03	7.64
(438 ppm)	0.870	702	3.43	4.73	6.87
	7.826	5791	3.51	4.68	6.96

908 [a]measured after concentration of samples in the rotavap.
909 [b]surface tension depression relative to water at T = 34 °C at a CWSOC = 1000 ppm.
910

Table 7: Molar mass uncertainty analysis and total uncertainty as percent of molar mass for the T1 site samples.

Sample	Uncertainty to σ (g mol^{-1})	Uncertainty to ω (g mol^{-1})	Uncertainty to υ_{org} (g mol^{-1})	Uncertainty to υ_{inorg} (g mol^{-1})	Uncertainty to ε_{org} (g mol^{-1})	Uncertainty to ε_{inorg} (g mol^{-1})	Total Uncertainty (%)
MEX-T1-1	0.105	4.813	15.749	20.892	0.0004	0[a]	14.5
MEX-T1-2	0.047	6.472	3.178	6.674	85.145	0[a]	44.0
MEX-T1-3	0.080	3.740	6.137	17.009	0.001	0[a]	10.8
MEX-T1-4	0.098	7.212	10.057	34.513	0.001	0[a]	22.3
MEX-T1-6	0.011	0.930	1.032	1.918	0[a]	0[a]	3.3
MEX-T1-7	N/A[b]	N/A[b]	N/A[b]	N/A[b]	N/A[b]	N/A[b]	N/A[b]
MEX-T1-8	0.109	21.291	29.332	96.639	0.001	0[a]	41.4
MEX-T1-9	0.082	15.620	23.676	93.514	0.002	0[a]	28.1
MEX-T1-10	0.045	7.776	16.986	50.696	0.001	0[a]	18.6
MEX-T1-11	0.019	5.316	6.871	19.369	0.001	0[a]	10.0
MEX-T1-12	0.244	5.872	9.498	28.946	0.001	0[a]	10.3

[a]Values are much smaller than 10^{-5} g mol^{-1}.
[b]N/A: Not available.

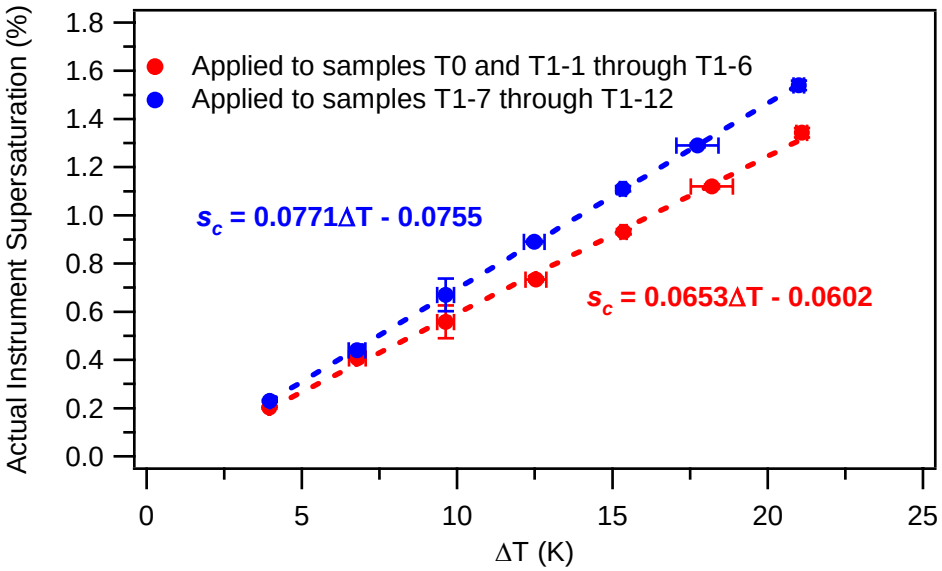
Actual Instrument Supersaturation (%)
1.8
1.6
1.4
1.2
1.0
0.8
0.6
0.4
0.2
0.0
Applied to samples T0 and T1-1 through T1-6
Applied to samples T1-7 through T1-12
s_c = 0.0771ΔT - 0.0755
s_c = 0.0653ΔT - 0.0602
0
5
10
15
20
25
ΔT (K)

Figure 1.

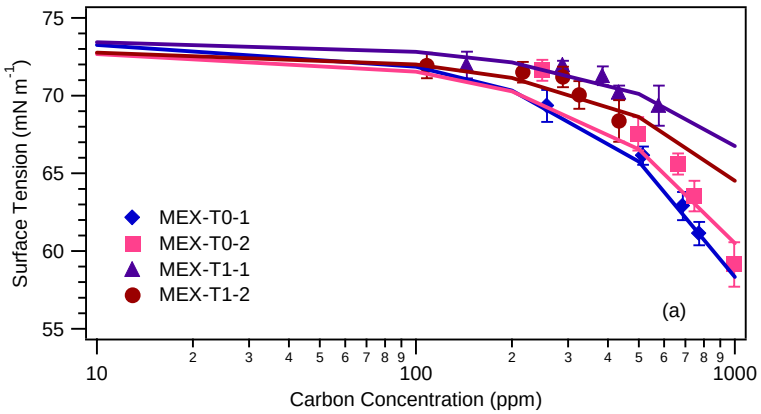
Surface Tension (mN m-1)
Carbon Concentration (ppm)
MEX-T0-1
MEX-T0-2
MEX-T1-1
MEX-T1-2
(a)

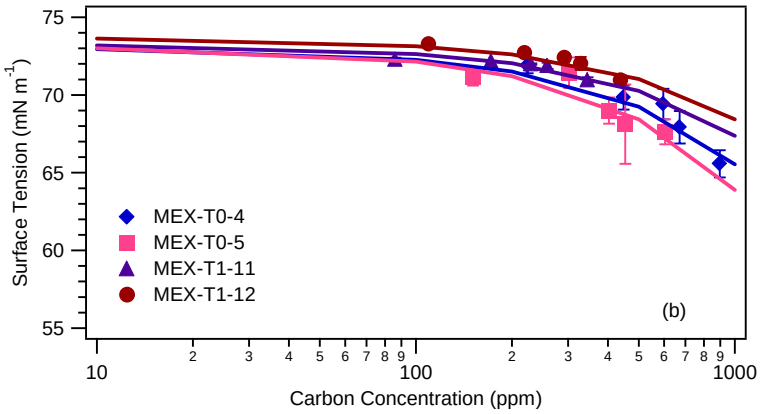
Surface Tension (mN m-1)
Carbon Concentration (ppm)
MEX-T0-4
MEX-T0-5
MEX-T1-11
MEX-T1-12
(b)

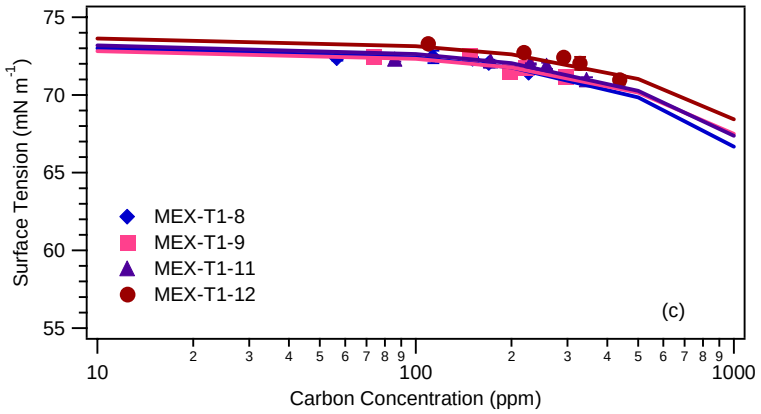
Surface Tension (mN m-1)
Carbon Concentration (ppm)
MEX-T1-8
MEX-T1-9
MEX-T1-11
MEX-T1-12
(c)

Figure 2.

947

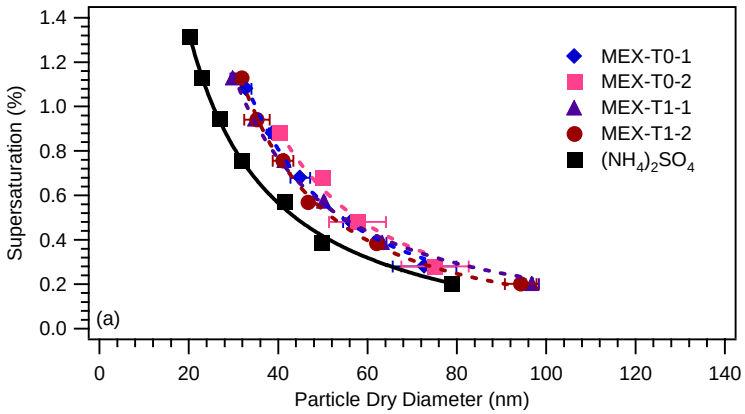

948

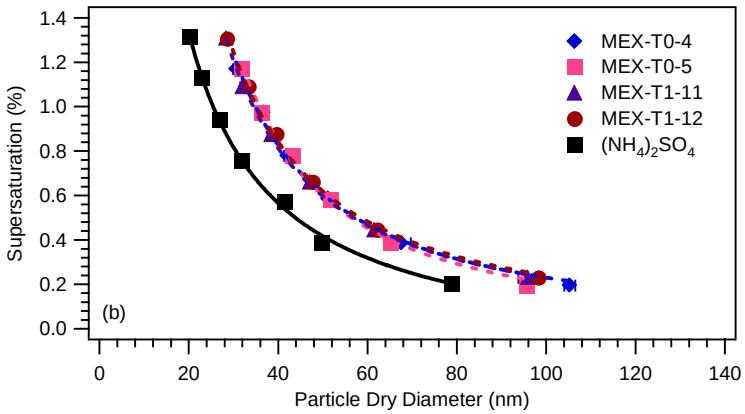

949

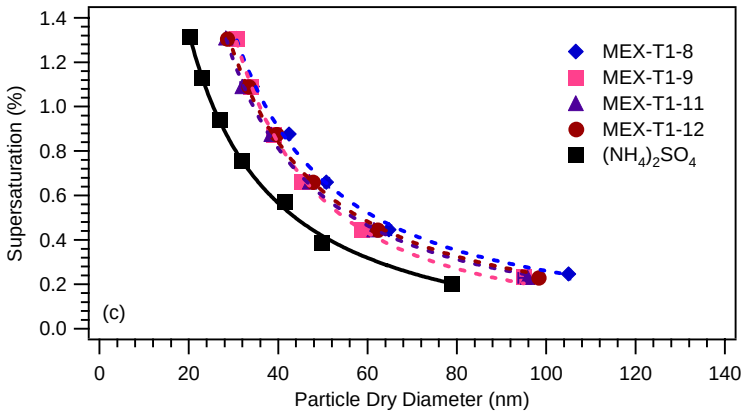

950

951 Figure 3.

952

953

954

955

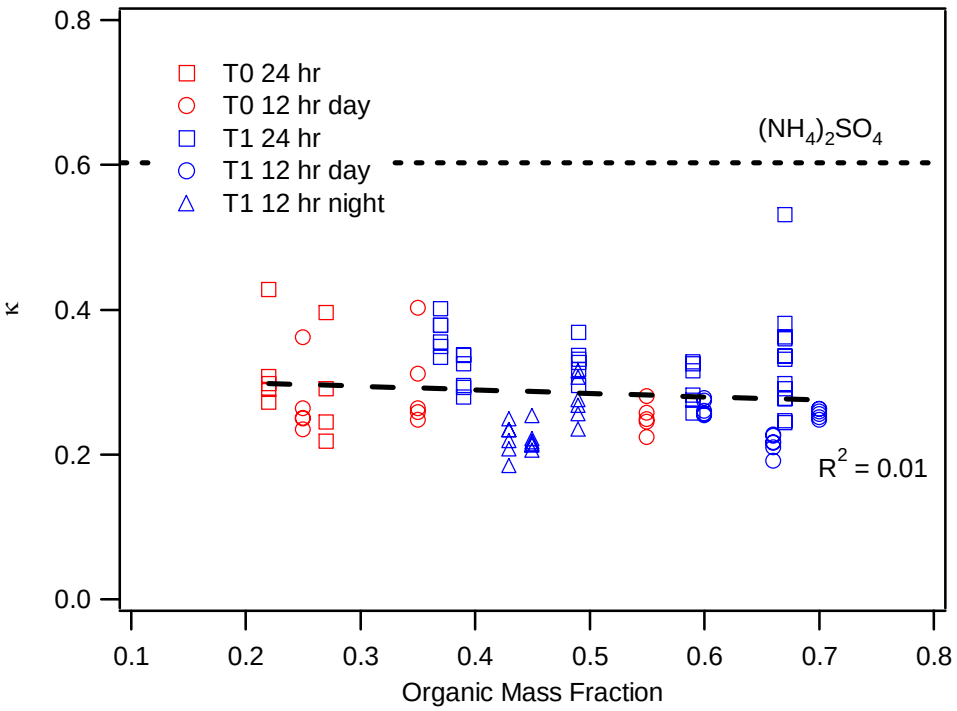
0.8
0.6
0.4
0.2
0.0
κ
T0 24 hr
T0 12 hr day
T1 24 hr
T1 12 hr day
T1 12 hr night
(NH4)2SO4
R2 = 0.01
0.1
0.2
0.3
0.4
0.5
0.6
0.7
0.8
Organic Mass Fraction

Figure 4.

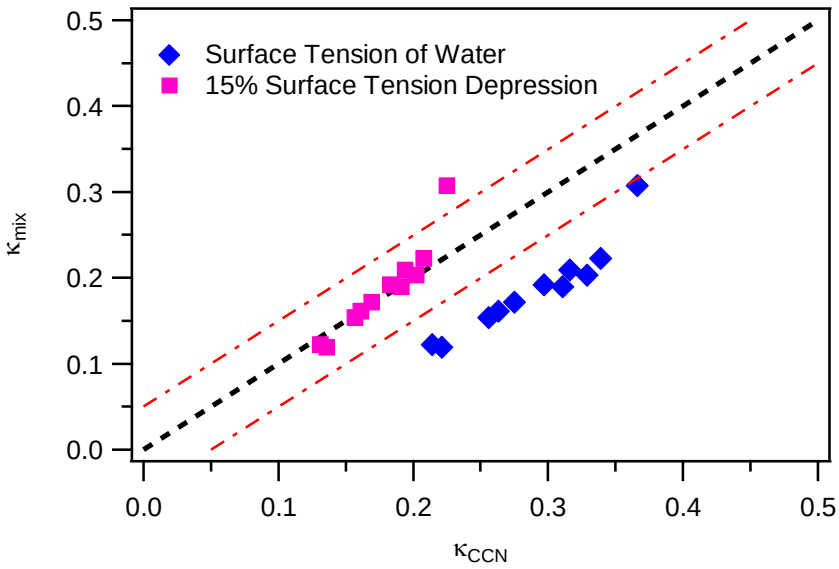

971
972

973 Figure 5.

974

975

976

977

978

979

980

981

982

983

984

985

986

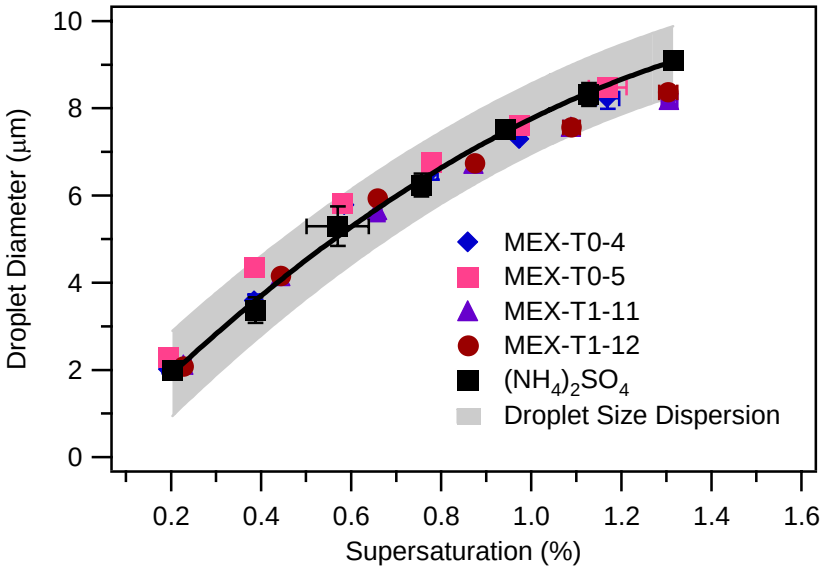
Droplet Diameter (µm)
Supersaturation (%)
MEX-T0-4
MEX-T0-5
MEX-T1-11
MEX-T1-12
(NH4)2SO4
Droplet Size Dispersion

Figure 6.